УДК 66

THE GAS-SOLID-SOLID PACKED CONTACTOR: MECHANISTIC AND MACROSCOPIC ANALYSIS OF THE INTERACTIVE FORCES

Marzouk Benali

Natural Resources Canada – CANMET Energy Technology Centre Varennes, Canada

Represented by a Member of Editorial Board Professor T.Kudra

Key words and phrases: Gas-solids direct contact; Dilute gas-solid suspension; Packed contactor; Interactive forces.

Abstract: Interactive forces between the three phases (gas, fine particles, and coarse and dense particles) govern the direct contact mechanism that occurs in the Gas-Solid-Solid Packed Contactor (**GSSPC**). Using continuity and momentum equations, these interactive forces are derived as functions of the overall pressure drop, the average dynamic hold up of solids, and the physical properties of solids, gas and a regular packing. Particle-packing walls collision model has been proposed to interpret the occurrence and physical origin of these interactive forces, to quantify them, and to predict the overall pressure drop in the three phases system.

Symbols

A_w – packed cross section (m^2);
a, a' – fitting parameters (-);
b, b' – fitting parameters (-);
D – internal diameter of column (m);
d – particle diameter (m);
$\overline{F}$ – average interactive force (N/m^3);
g – gravitational acceleration (m^2/s);
k_v – proportionality factor between the dynamic hold-up of the solids in the vicinity of the packing walls and the particle-packing walls collision frequency (-);
L – length (m);
m – mass of particle (kg);
P – pressure (Pa);
r – radial direction (m);
t_p – residence time of the particle p before collision (s);
V_f – gas superficial velocity (m/s);
$\left(V_p^{lat}\right)_x^{inc}$ – particle velocity before lateral collision in axial direction (m/s);
$\left(V_p^{lat}\right)_x^{ref}$ – particle velocity after lateral collision in axial direction (m/s);
$\left(V_p^{lat}\right)_r^{inc}$ – particle velocity before lateral collision in radial direction (m/s);
$\left(V_p^{lat}\right)_r^{ref}$ – particle velocity after lateral collision in radial direction (m/s);
$\left(V_p^{fr}\right)_r^{inc}$ – particle velocity before frontal collision in radial direction (m/s);
$\left(V_p^{fr}\right)_r^{inc}$ – particle velocity after frontal collision in radial direction (m/s);
W – mass flow rate of solids (kg/s);
x – axial direction.

Greek letters

$\alpha_i\left(x,t\right)$ – instantaneous dynamic hold-up of phase i (-);
$\overline{\alpha}_i$ – average dynamic hold-up of phase i (-);
ΔE_{kin} – change of kinetic energy (J);
Δt_{sv} – closing-opening time (s);
Γ_{pw} – momentum loss of particle, due to particle-wall collisions;
Γ_z – momentum received by zirconia particle, due to particle-particle collisions (kg·m/s);
Π_{pw} – frequency of collisions between particles and packing walls;

ε_{pc} – packing void fraction (-);
λ – coefficient of restitution (-);
μ – dynamic viscosity (kg/m.s);
ρ – density (kg/m^3).

Subscripts

coll – collision;
f – gas;
n – normal;
p – particle;
pc – packing;
r – radial;
s – sand;
t – tangential;
w – walls;
x – axial;
z – zirconia;
zs – zirconia-sand.

Superscripts

eff – effective;
fr – frontal;
inc – incident;
lat – lateral;
ref – reflected;
(0) – air without solids;
(1) – air-sand system;
(2) – air-zirconia system;
(3) – air-sand-zirconia system.

1 Introduction

Direct contact of phases in gas-solid mixtures is frequently encountered in many industrial and engineering applications, as well as in a certain number of natural phenomena that occur, for example, in chemical reactors, pneumatic conveying, divided solid waste treatment, and heat recovery from hot solids. Several authors [1-5] have demonstrated that gas-solid, solid-solid and solid-wall interaction forces play important roles in such applications because they directly affect circulation of solids and transfer of heat to the particles and the packing walls comprising both internal and external walls of the packing element.

An understanding of the hydrodynamics of direct contact mechanisms occurring in the Gas-Solid-Solid Packed Contactor (GSSPC) can greatly facilitate comprehension of the basic aspects of the physical mechanisms involved, and predicting of heat transfer mechanisms in applications of GSSPC related to heat recovery from hot solids. Studies of the behavior of gas-solid mixtures by Wang [6], Arastoopour et al. [7-9], Fan et al. [10], Satija and Fan [11], Saatdjian and Large [12, 13], Gwyn [14] and Gidaspow [15] have resulted in numerous analytical and numerical models for calculating the gas-solid interactive force and the particle-particle interaction coefficient based on the drag concept and/or the Ergun's Equation. Saatdjian and Large [12, 13] assumed a negligible pressure drop for the gas flowing along the packed column. In addition, they introduced an effective volumetric concentration of the solids to calculate the gas-solid interactive force as the pressure drop per unit volume given by the Ergun's Equation. Unfortunately, these models were based on a number of assumptions that oversimplified certain physical phenomena inherent in such operations, namely: interphase mass/heat transfer and particle-wall friction are not considered, velocity field is uniform, and the total voidage is used for drag force expressions.

In addition, popularization of the mechanics of a continuous medium has led many researchers [16-19] to apply the kinetic theory of gases to granular flow in order to clarify various physical concepts (e.g. viscosity and solids pressure), and to use the theory of molecular collision to formulate and compute the external forces involved in multiphase flow.

Further work on the phase presence probability in gas-solid mixtures and the phenomena occurring at the interfaces between phases inspired Molodtsof and Muzyka [20] to describe the gas-solid suspension flow based on a rigorous mathematical model. The model is governed by a probabilistic concept describing the random motion of each solid phase. The authors considered that the hold-up presence and velocity of a given phase at a given point and time were random and followed probability laws. Because the external forces acting on gas phases are different from those acting on solid phases, Molodtsof and Muzyka [20] considered them separately. Mathematical treatment of the external forces

acting on each phase in a multiphase mixture made it possible not only to identify all forces, but also to clearly understand their physical origins. Fortier [17] is generally credited as the first who used the phase presence probability concept as a basis for the hydrodynamic understanding and modeling of the gas-solid suspension flow.

This paper focuses on a theoretical analysis, based on general momentum equations, of the direct contact mechanism between the upward flow of a gas-solid suspension, and trickling of coarse and dense particles. Such a hydrodynamic analysis of the mechanisms occurring in the GSSPC makes it possible to forecast:

– the overall pressure drop of a given industrial installation, with a view to sizing and selecting the blowing equipment; and

– the solid concentration in the packed effective zone, which controls the performance of the GSSPC when it is operated as a heat exchanger.

2 Description of the gas-solid-solid packed contactor

As illustrated in Fig. 1, the GSSPC consists of a packed bed section having an internal diameter and length of 114 and 700 mm, respectively. Cylindrical Pall rings (25 mm-internal diameter) are used as the packing in a regular arrangement. The packing slows down the trickling of solid particles and thus creates a greater hold-up of particles than an empty column. When the GSSPC operates as a heat exchanger, a significant longitudinal temperature gradient for the solid phase appears because temperature is inversely proportional to the trickling velocity of particles. In addition, the packing plays an essential role in maintaining a uniform distribution of the solid particles through the effective section of the GSSPC, while opposing any form of radial segregation. However, at high gas velocity (U > 9 m/s), the experimental results showed the phenomena of incipient choking, and incipient radial and axial segregation [21]. The principle of operation is based on a vertical pneumatic transport of fine particles (sand particles, with an average diameter of 179 μm), a trickle flow of coarse and dense particles (zirconia particles, with an average diameter of 1,320 μm), and a gas-solid separation.

Table 1

Physical properties of solid particles

	$d_i\,(m)\times 10^6$	$\rho_i\left(kg/m^3\right)$
Sand	179	2646
Zirconia	1320	3774

The fine particles are introduced into the packed section by a conical ejector. The coarse and dense particles are transported using a screw elevator. In order to prevent short-circuiting of the gas through the return line of the coarse and dense particles, a gas-lock is installed at the bottom of the standpipe. Two pneumatically actuated slide valves are placed in the packed section. In the open position, the valves are "full bore" so as not to affect the flow patterns of the solids and gases. Inflatable rubber gaskets ensure airtightness. Considerable care is taken to ensure simultaneous closing of the two slide valves. The mean volumetric solids concentration is determined on the basis of the mass of solids recovered when the slide valves are closed.

The distance between the two slide valves is 700 mm; the inside pipe diameter is 114 mm. A detailed description of the operation of GSSPC can be found in [21].

The mean solids concentration is then given by:

$$\bar{\alpha}_j = \frac{4 m_{sv}}{\pi \rho_j \varepsilon_{pc} D^2 H_{pc}}. \qquad (1)$$

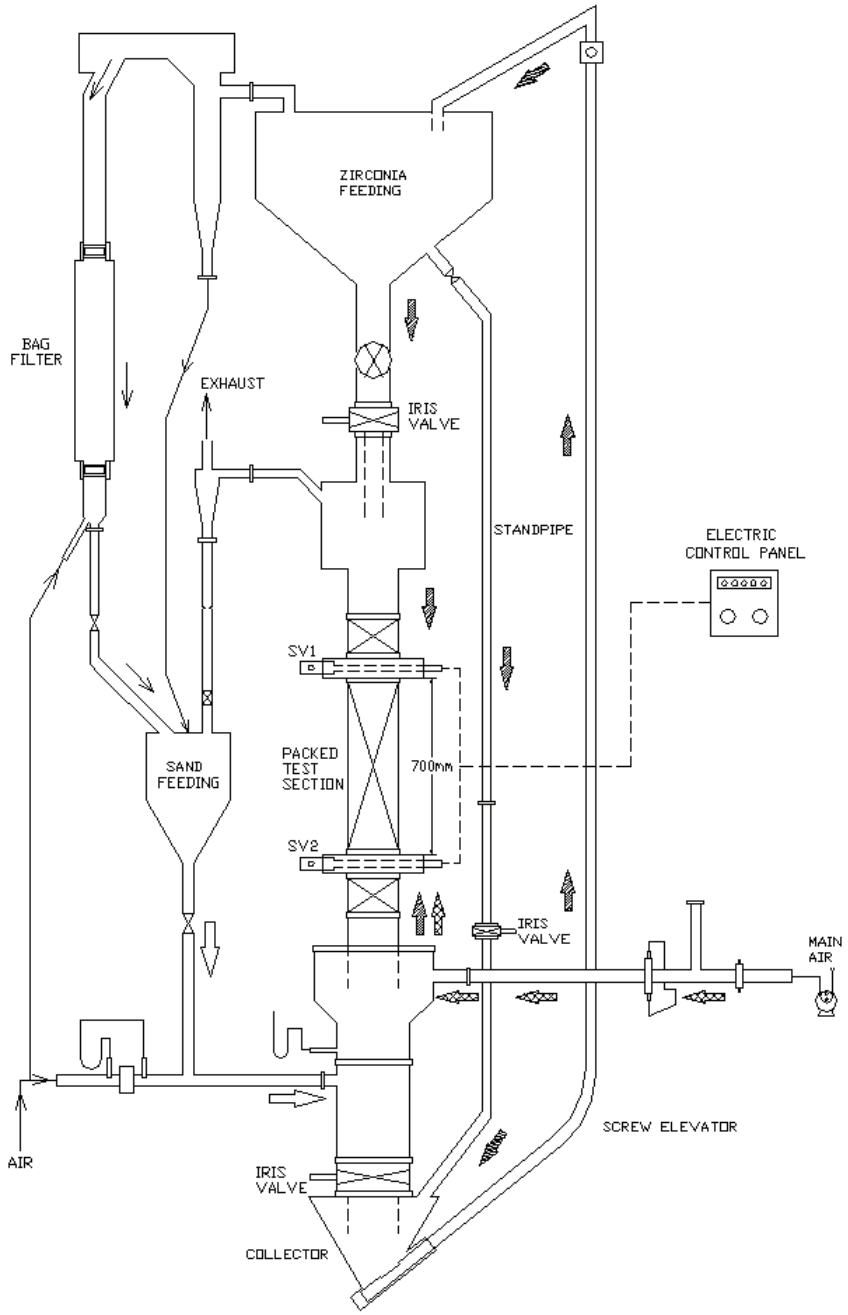

Fig. 1 Gas-Solid-Solid Packed Contactor: General view of pilot-scale unit

For the two and three-phase flows, Eq. (1) can be written respectively:

$$\bar{\alpha}_j = \frac{4 m_{sv}}{\pi \rho_j \left(\varepsilon_{pc} - \bar{\alpha}_i \right) D^2 H_{pc}} \tag{2}$$

and

$$\bar{\alpha}_k = \frac{4 m_{sv}}{\pi \rho_k \left(\varepsilon_{pc} - \bar{\alpha}_i - \bar{\alpha}_j \right) D^2 H_{pc}} . \tag{3}$$

The maximum error involved in the measurement of the average solids concentration is estimated based on the following assumptions: when the lower slide valve closes first, the solid particles of a phase (i) continue to leave the test section at the flow rate W_i during the time interval Δt_{sv}. This interval is the elapsed time before the upper valve is closed. Similarly, when the upper slide valve is first to close, the solids continue to flow into the packed test section at the flow rate W_i during the time Δt_{sv}. The difference between the measured and real values of the solids concentration is then given by:

$$\Delta\bar{\alpha}_i = \left(\frac{4W_i}{\pi\rho_i \varepsilon_{pc} D^2 H_{pc}} \right) \Delta t_{sv} . \tag{4}$$

Since the distribution of the solid particles is uniform in the packed section, the percentage error is given as follows:

$$\frac{\Delta\bar{\alpha}_i}{\bar{\alpha}_i}(\%) = \left(\frac{\bar{V}_i}{H_{pc}} \right) \Delta t_{sv} \times 100 . \tag{5}$$

In general, the time interval Δt_{sv} is less than 5 milliseconds. The maximum errors are thus generally less than 5 %.

3 Basic flow equations

The present analysis examines the packed test section of the GSSPC as a multiphase medium, which is a heterogeneous mixture of non-miscible phases (a phase is considered here to be a component of the mixture that is mechanically separable from other components). The theoretical treatment of this multiphase medium is based on the concept of the phase presence probability in description of the gas-solid suspension flows. To describe the behavior of this multiphase medium, it is necessary to consider each phase separately since the interaction between all the phases in the gas-solid mixture will depend on the physical characteristics of each phase. Otherwords, if the distribution of species i in the mixture is assumed to be uniform, the phase presence probability $\alpha_i(x, t)$ will be non-variable with the time and the space co-ordinate:

$$\alpha_i(x,t) \equiv \bar{\alpha}_i . \tag{6}$$

As the solid particles penetrate a given packing stage of the effective contacting zone, they are rapidly slowed down due to collisions with the packing walls, and their mean velocity becomes independent of the space co-ordinate. When the solid particles enter and exit the packing test section, their velocity can be changed. Thus, a small packed column is added each side of the effective test section of the GSSPC to prevent entry and exit effects (Fig. 2). Therefore, the multiphase flow (air as a gas-phase, sand and zirconia as the solid-phases) is considered to be in a steady state, viz. the rate of momentum change for the phase "i" in the mixture is zero.

Under these conditions, the flow equations for each phase in the gas-sand-zirconia system are formulated as follows:

3.1 Counter-current trickle flow of zirconia particles and fine particle suspension

Gas phase

$$-\bar{\alpha}_f^{(3)} \left(\frac{dP}{dx} \right)_T^{(3)} - \bar{\alpha}_f^{(3)} \rho_f g - \bar{F}_{wf}^{(3)} - \bar{F}_{fs}^{(3)} - \bar{F}_{fz}^{(3)} = 0 \tag{7}$$

Sand phase

$$-\bar{\alpha}_s^{(3)} \rho_s g - \bar{\alpha}_s^{(3)} \left(\frac{dP}{dx} \right)_T^{(3)} - \bar{F}_{ws}^{(3)} + \bar{F}_{fs}^{(3)} - \bar{F}_{zs}^{(3)} = 0 . \tag{8}$$

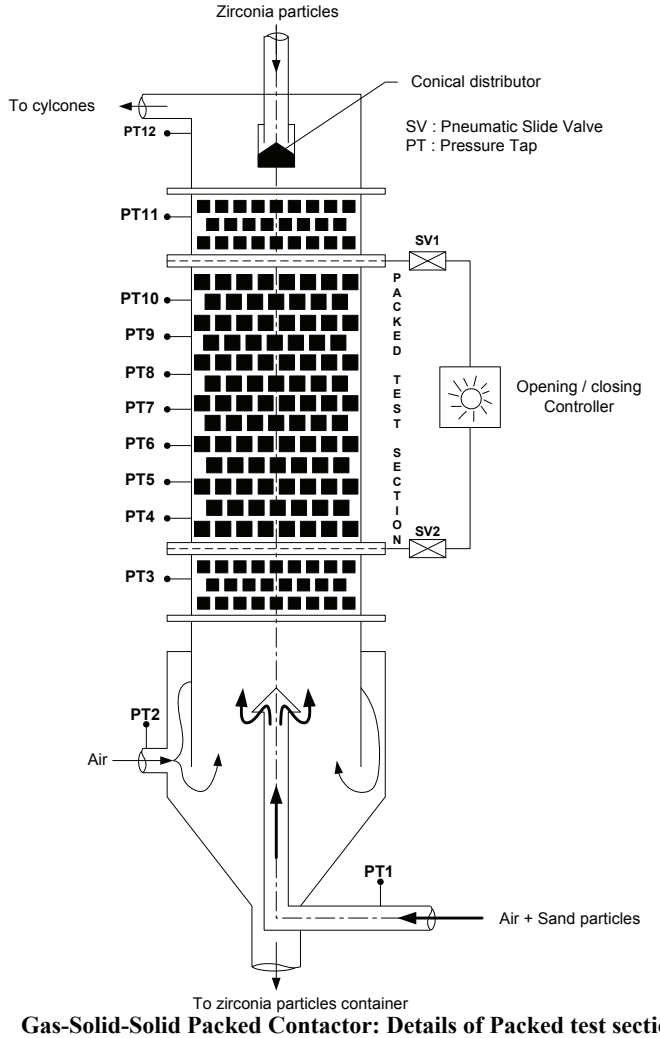

Fig. 2 Gas-Solid-Solid Packed Contactor: Details of Packed test section

Zirconia phase

$$-\bar{\alpha}_z^{(3)}\rho_z g - \bar{\alpha}_z^{(3)}\left(\frac{dP}{dx}\right)_T^{(3)} + \bar{F}_{wz}^{(3)} + \bar{F}_{fz}^{(3)} + \bar{F}_{zs}^{(3)} = 0 \ . \qquad (9)$$

The above system of equations highlights several unknown variables:

1. the average dynamic hold-up of each phase $\bar{\alpha}_f^{(3)}$, $\bar{\alpha}_s^{(3)}$, $\bar{\alpha}_z^{(3)}$;
2. the overall pressure *P*;
3. the gas-solids interactive forces $\bar{F}_{fs}^{(3)}$, $\bar{F}_{fz}^{(3)}$;
4. the gas-walls and solids-walls interactive forces $\bar{F}_{fw}^{(3)}$, $\bar{F}_{sw}^{(3)}$, $\bar{F}_{zw}^{(3)}$; and
5. the solid-solid interactive forces $\bar{F}_{zs}^{(3)}$, which translates into the total force under consideration.

Among these unknown variables, $\bar{\alpha}_s^{(3)}$, $\bar{\alpha}_z^{(3)}$ and *P* are measurable. The relationship between these measurable variables can be derived in the form of the following expression:

$$\left(\frac{dP}{dx}\right)_T^{(3)} = -\frac{1}{\varepsilon_{pc}} \left\{ \left[\varepsilon_{pc}\rho_f + \left(\rho_s - \rho_f\right) \bar{\alpha}_s^{(3)} + \left(\rho_z - \rho_f\right) \bar{\alpha}_z^{(3)} \right] g + \bar{F}_{wf}^{(3)} + \bar{F}_{ws}^{(3)} - \bar{F}_{wz}^{(3)} \right\}. \tag{10}$$

Solving Eqs. (7), (8) and (9) thus requires a separate analysis of the hydrodynamic behavior of the air-sand and air-zirconia flows as well as a mechanistic analysis of the collisions between sand and zirconia particles, and between solid particles and packing walls.

3.2 Co-current upward flow of sand particles and gas

Gas phase:

$$-\bar{\alpha}_f^{(1)} \left(\frac{dP}{dx}\right)_T^{(1)} - \bar{\alpha}_f^{(1)} \rho_f g - \bar{F}_{wf}^{(1)} - \bar{F}_{fs}^{(1)} = 0 \ . \tag{11}$$

Sand phase:

$$-\bar{\alpha}_s^{(1)} \left(\frac{dP}{dx}\right)_T^{(1)} - \bar{\alpha}_s^{(1)} \rho_s g - \bar{F}_{ws}^{(1)} + \bar{F}_{fs}^{(1)} = 0 . \tag{12}$$

Knowing that $\bar{\alpha}_f^{(1)} + \bar{\alpha}_s^{(1)} = 1 - \bar{\alpha}_{pc} = \varepsilon_{pc}$, combining Eqs. (11) and (12) gives:

$$\bar{F}_{fs}^{(1)} = -\left(\varepsilon_{pc} - \bar{\alpha}_s^{(1)}\right) \left[\left(\frac{dP}{dx}\right)_T^{(1)} + \rho_f g \right] - F_{wf}^{(1)} \ ; \tag{13}$$

$$\bar{F}_{ws}^{(1)} = -\varepsilon_{pc} \left(\frac{dP}{dx}\right)_T^{(1)} - \left[\varepsilon_{pc}\rho_f + \bar{\alpha}_s^{(1)} \left(\rho_s - \rho_f\right) \right] g - \bar{F}_{wf}^{(1)} . \tag{14}$$

Force $\bar{F}_{wf}^{(1)}$ can be deduced from the reference flow, which corresponds to the flow of the gas without solids. The overall pressure drop in the gas flowing alone, undisturbed by the presence of solid particles, is given by the Navier-Stokes equation integrated over the packed cross-section:

$$-\bar{\alpha}_f^{(0)} \left(\frac{dP}{dx}\right)_T^{(0)} = \bar{\alpha}_f^{(0)} \rho_f g + \bar{F}_{wf}^{(0)} . \tag{15}$$

The superscript (0) refers to the gas flowing alone at the same superficial velocity in the presence of solid particles.

Since:

$$\bar{\alpha}_f^{(0)} = 1 - \alpha_{pc} = \varepsilon_{pc} . \tag{16}$$

Thus:

$$\bar{F}_{wf}^{(0)} = -\varepsilon_{pc} \left(\rho_f g + \left(\frac{dP}{dx}\right) \right)_T^{(0)} . \tag{17}$$

With the addition of the solid phase, the perturbation method for a given steady flow allows the flowing suspensions to be compared to the reference flow, and the gas-wall interaction is given as follows:

$$\bar{F}_{wf}^{(1)} = \bar{F}_{wf}^{(0)} + \bar{\alpha}_s^{(1)} \left(\bar{F}_{wf}^{(0)} \right). \tag{18}$$

Since the dilute suspensions are defined as those that satisfy the condition $\bar{\alpha}_s^{(1)} \langle\langle 1$,

Eq. (18) might be simplified to:

$$\bar{F}_{wf}^{(1)} \approx \bar{F}_{wf}^{(0)}. \tag{19}$$

This simplification is supported also by the Einstein's classical analysis on the viscosity of an infinitely dilute suspension of solid spheres [23, 24], which defines the apparent viscosity as:

$$\mu = \mu_0 \left(1 + 0\left(\bar{\alpha}\right)\right). \tag{20}$$

Here, the apparent viscosity is composed of the viscosity of the fluid in the absence of particles and a perturbation term of the order of magnitude of the volumetric solid concentration. Jeffrey and Acrivos (25) obtained the same results in their experimental and theoretical work on the rheological properties of gaseous suspensions of rigid particles. Accordingly, Eqs. (13) and (14) can be transformed as follows:

$$\bar{F}_{fs}^{(1)} = -\varepsilon_{pc}\left[\left(\frac{dP}{dx}\right)_T^{(1)} - \left(\frac{dP}{dx}\right)_T^{(0)}\right] + \bar{\alpha}_s^{(1)}\left[\left(\frac{dP}{dx}\right)_T^{(1)} + \rho_f g\right]; \tag{21}$$

$$\bar{F}_{ws}^{(1)} = -\varepsilon_{pc}\left[\left(\frac{dP}{dx}\right)_T^{(1)} - \left(\frac{dP}{dx}\right)_T^{(0)}\right] - \bar{\alpha}_s^{(1)}\left(\rho_s - \rho_f\right)\ g. \tag{22}$$

3.3 Counter-current trickle flow of zirconia particles and gas

While proceeding with the same analytical approach, the flow equations of the *air-zirconia system* can be written as follows:

Gas phase:

$$-\bar{\alpha}_f^{(2)}\left(\frac{dP}{dx}\right)_T^{(2)} - \bar{\alpha}_f^{(2)}\rho_f g - \bar{F}_{wf}^{(2)} - \bar{F}_{fz}^{(2)} = 0. \tag{23}$$

Zirconia phase:

$$-\bar{\alpha}_z^{(2)}\left(\frac{dP}{dx}\right)_T^{(2)} - \bar{\alpha}_z^{(2)}\rho_z g + \bar{F}_{wz}^{(2)} + \bar{F}_{fz}^{(2)} = 0. \tag{24}$$

As in the previous case, generalization of Einstein's rheological approach to a dilute suspension of solid spheres gives:

$$\bar{F}_{wf}^{(2)} = \bar{F}_{wf}^{(0)}\left(1 + 0\ \ \left(\bar{\alpha}_z\right)\right). \tag{25}$$

Consequently:

$$\bar{F}_{fz}^{(2)} = -\varepsilon_{pc}\left[\left(\frac{dP}{dx}\right)_T^{(2)} - \left(\frac{dP}{dx}\right)_T^{(0)}\right] + \bar{\alpha}_z^{(2)}\left[\left(\frac{dP}{dx}\right)_T^{(2)} + \rho_f g\right]; \tag{26}$$

$$\bar{F}_{wz}^{(2)} = \varepsilon_{pc}\left[\left(\frac{dP}{dx}\right)_T^{(2)} - \left(\frac{dP}{dx}\right)_T^{(0)}\right] + \bar{\alpha}_z^{(2)}\left(\rho_z - \rho_f\right)\ g. \tag{27}$$

Due to the low particle concentration within the packed test section, it is reasonable to assume that the addition of a second or third phase respectively in a single or two-phase flow system only introduces the additional interactive terms without significantly changing the interactive forces that already exist in the single or two-phase flow system. Indeed, the average dynamic hold-up of sand particles was in the range from 9.67×10^{-4} to 64.46×10^{-4} range in the *air-sand system*, and from 41.65×10^{-4} to 97.25×10^{-4} in the *air-sand-zirconia*

system, resulting in an increase from 0.01 to 0.64 % in the fluid-wall interactive forces. In the case of the *air-zirconia system*, the average dynamic hold-up of zirconia particles varied from 7.17×10^{-3} to 74.60×10^{-3}, whereas in the *air-sand-zirconia system*, this range spanned from 9.38×10^{-3} to 132.25×10^{-3}, resulting in an increase from 0.22 to 6.94 % in the fluid-packing walls interactive forces. Such analysis of the magnitude of variation in interactive forces due to additional phases gives supports the assumptions made concerning the dilute suspension effects. As indicated above, solid concentrations were assumed to be uniform in the packed test section. Radial concentration profile measurements were carried out using isokinetic probes inserted at the top and bottom of the packed test section. Figs 3 and 4 indicate only slight variations in radial concentration for both solids: in the *air-sand* and *air-sand-zirconia systems*, radial sand concentrations deviate about 0.4 to 3 % from the optimum value. In the *air-zirconia system* and *air-sand zirconia system*, deviations in radial zirconia concentrations from the optimum value are of the order of 1 to 7 %. The assumption that the concentration profiles of solids are uniform is therefore consistent with

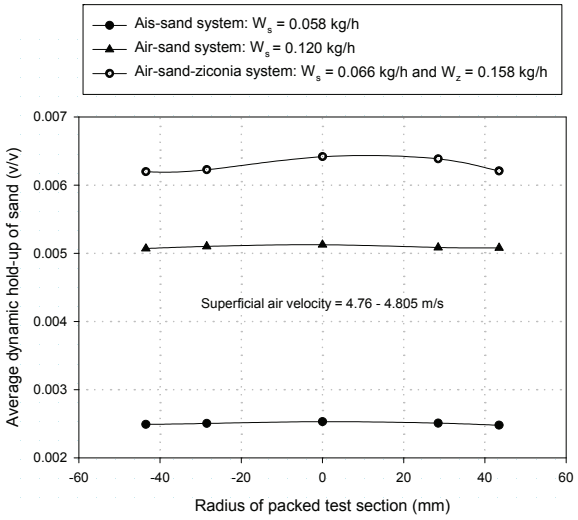

Fig. 3 Radial profile of sand volumetric concentration for a given sand mass flow rate

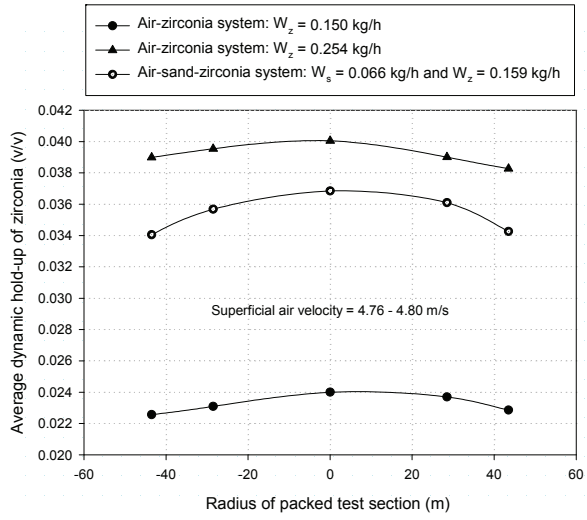

Fig. 4 Radial profile of zirconia volumetric concentration for a given ziconia mass flow rate

experimental results. Eq. (10), describing the expected overall pressure drop in a dilute tri-phase system, can thus be written as follows:

$$\left(\frac{dP}{dx}\right)_T^{(3)} = -\frac{1}{\varepsilon_{pc}}\left\{\left[\varepsilon_{pc}\rho_f + \left(\rho_s - \rho_f\right)\ \bar{\alpha}_s^{(3)} + \left(\rho_z - \rho_f\right)\ \bar{\alpha}_z^{(3)}\right]\ g + \bar{F}_{wf}^{(0)} + \bar{F}_{ws}^{(1)} - \bar{F}_{wz}^{(2)}\right\}. \tag{28}$$

4 Results and discussion

Eqs. (21), (22), (26) and (27) show that the average interactive forces per unit volume may be determined from the pressure-drop and average dynamic hold-up measurements in two-phase systems. These forces will be reported as a function of operating parameters (V_f, W_s, and W_z) considered as independent variables.

4.1 Gas-solid interactive forces

The curves shown in Figs. 5 and 6 for a given mass flow rate of solids show a systematic linear variation in the interactive forces as a function of relative velocity. Furthermore, the slopes of the curves in Figs. 4 and 5 increase (cf. Figs. 7 and 8) over the entire range of the solids mass flow rates. The experimental results may be correlated as follows:

$$\bar{F}_{fs}^{(1)} = a_{fs} V_{fs}, \text{ where } a_{fs} = -2.98\times10^5\, W_s^2 - 7.61\times10^{10}\, W_s - 1.51\times10^{-4}; \tag{29}$$

$$\bar{F}_{fz}^{(2)} = a_{fz} V_{fz}, \text{ where } a_{fz} = -16.87\times10^5\, W_z. \tag{30}$$

4.2 Solids-packing walls interactive forces

Based on the experimental results [13] obtained using the pilot-unit described in section 2, Figs. 9 and 10 show a linear variation of these interactive forces with increasing gas superficial velocity, for a given mass flow rate of solids. Analyses of these data yield the linear correlations described by Eqs. (31) and (32):

$$\bar{F}_{ws}^{(1)} = a_{ws} V_f, \text{ where } a_{ws} = -6.78\times10^{10}\, W_s^2 - 8.98\times10^5\, W_s - 0.32; \tag{31}$$

$$\bar{F}_{wz}^{(2)} = a_{wz} V_f, \text{ where } a_{wz} = 62.58\times10^5\, W_z. \tag{32}$$

The slopes of the curves in Figs. 9 and 10 also vary linearly as a function of the mass flow rate of solids, (cf. Figs. 11 and 12).

These two correlations could be rewritten in the following form:

$$\frac{\bar{F}_{wz}^{(2)}}{\bar{F}_{ws}^{(1)}} = -\ \frac{62.58\times10^5\, W_z}{6.78\times10^{10}\, W_s^2 + 8.98\times10^5\, W_s + 0.32}. \tag{33}$$

The negative sign in Eq. (33) reflects the fact that interactive forces F_{ws} and F_{wz} are in opposite directions. For a constant mass flow rate of zirconia particles, Eq. (33) shows that, as the mass flow rate of sand particles increases, the interactive forces between the packing walls and zirconia particles decrease; viz. the trickles sliding over the packing are slowed down by the upward flow of the sand particles. We now can confirm that the presence of sand particles increases the average dynamic hold-up of zirconia particles in the packed test section of the GSSPC.

4.3 Particle-particle interactive forces

For a given gas superficial velocity and a given mass flow rate of zirconia particles, an increase in the mass flow rate of sand results in a decrease in the interactive force between zirconia and sand particles The results depicted in Fig. 13 provide further evidence

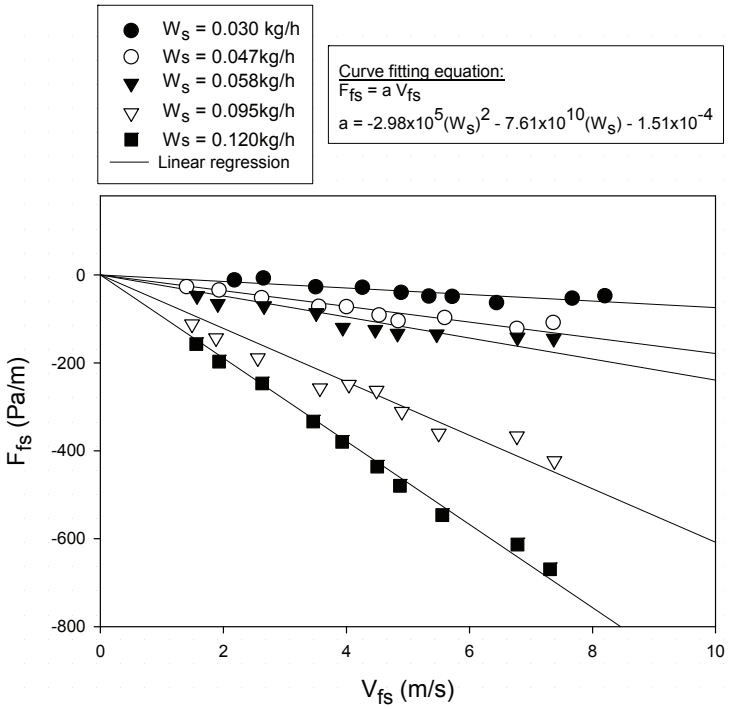

Fig. 5 Gas-sand interactive forces as a function of relative velocity

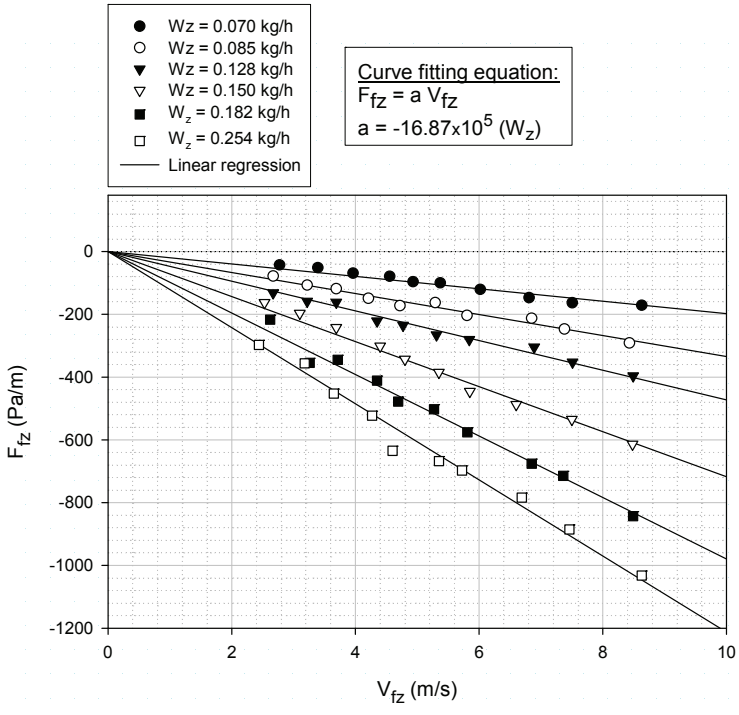

Fig. 6 Gas-zirconia interactive forces as a function of relative velocity

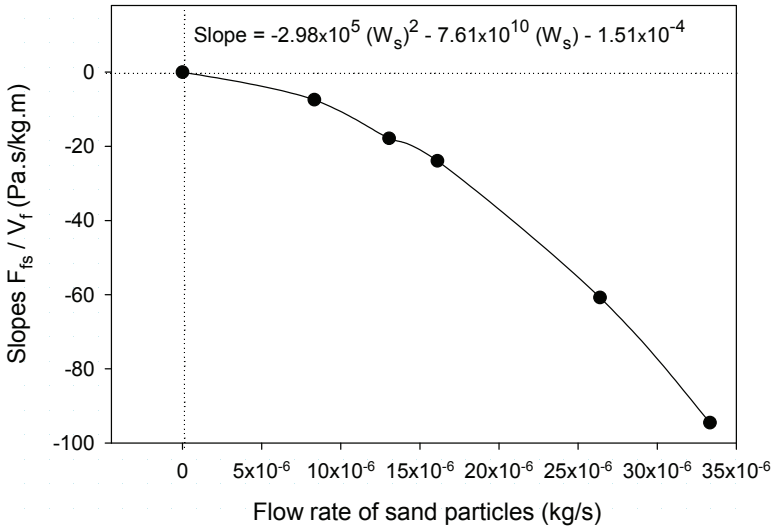

Fig. 7 Slopes of gas-sand interactive forces as a function of sand mass flow rate

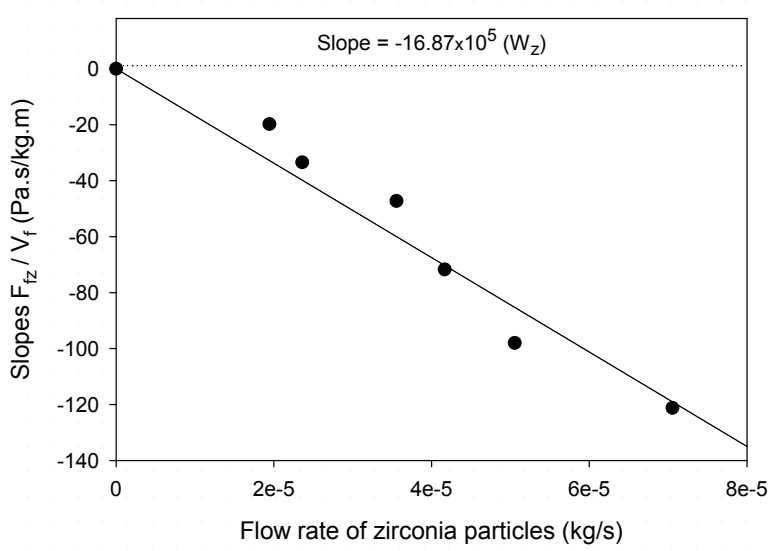

Fig. 8 Slopes of gas-zirconia interactive forces as a function of zirconia mass flow rate

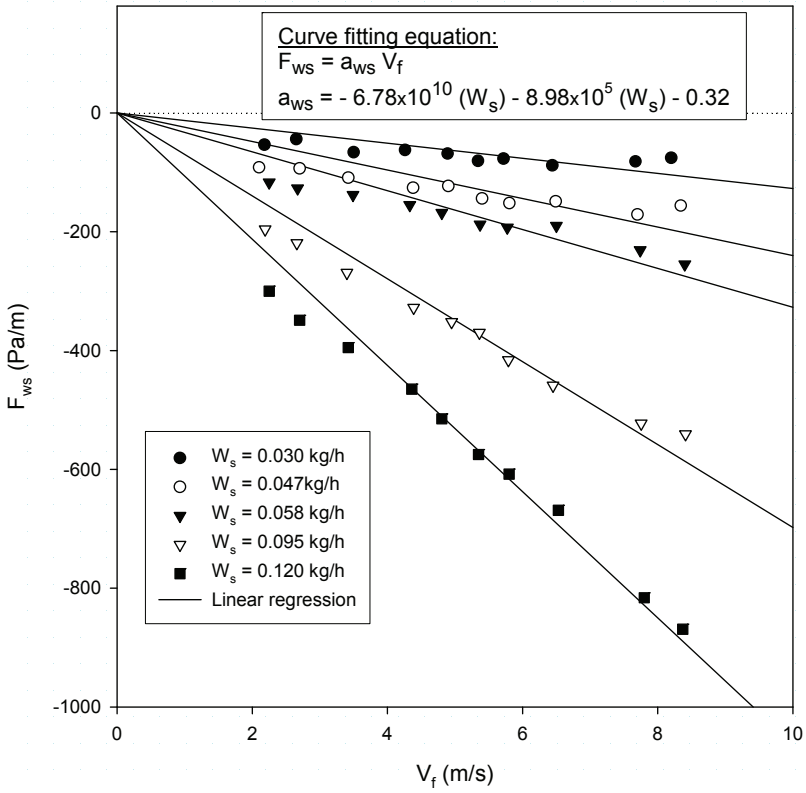

Fig. 9 Sand-wall interactive forces as a function of gas superficial velocity

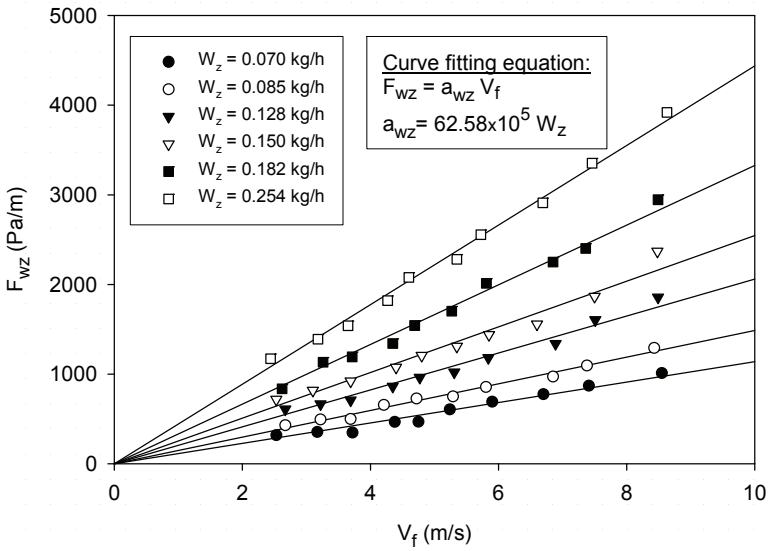

Fig. 10 Zirconia-wall interactive forces as a function of gas superficial velocity

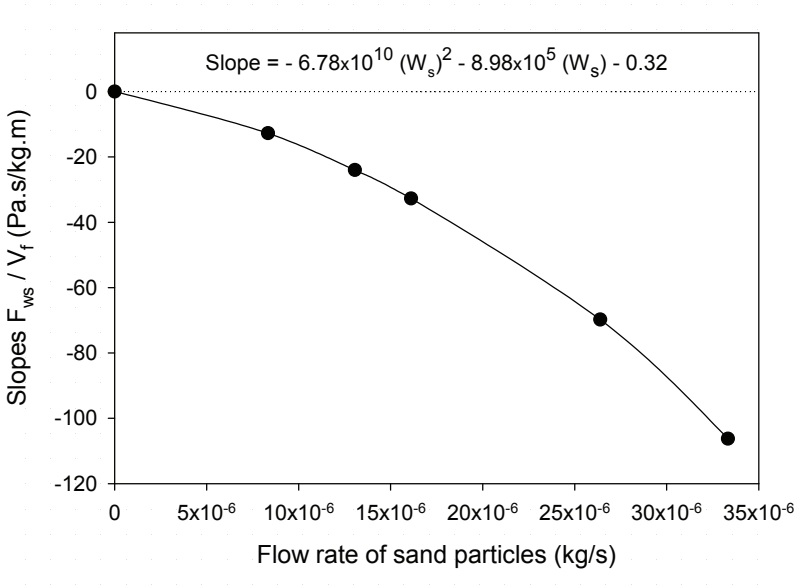

Fig. 11 Slopes of sand-wall interactive forces as a function of sand mass flow rate

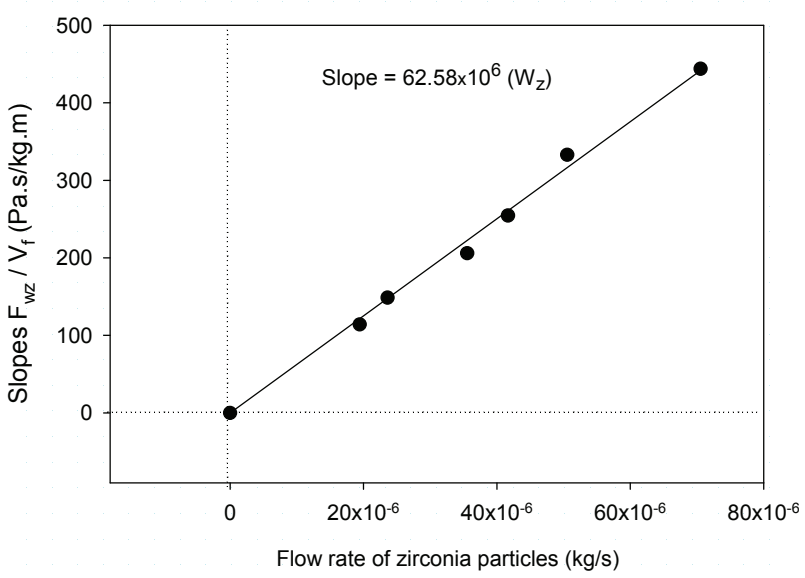

Fig. 12 Slopes of zirconia-wall interactive forces as a function of zirconia mass flow rate

presented in previous work [20] that, for a relatively low mass flow rate of sand particles, the trickle flow of zirconia particles is also relatively low. On the other hand, Fig. 13 shows a linear increase of particle-particle interaction with gas superficial velocity. This suggests the existence of two flow zones:

Zone I: The force F_{zs} is in the direction of zirconia particle trickles, viz. the sand particle effect of increasing the zirconia particle hold-up is very low in this region.

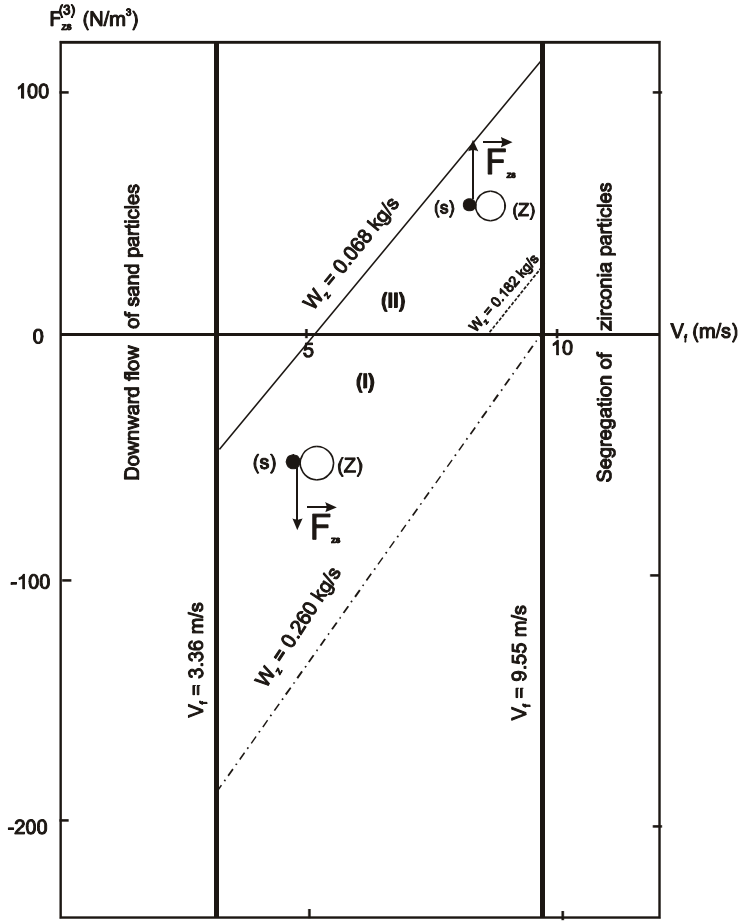

Fig. 13 Flow diagram showing the effect of direct mechanical interaction between two solid phases

Zone II: *T*he force F_{zs} is in the direction of upward stream of air, viz. the zirconia particles are moving slowly and therefore an increase in their average dynamic hold-up is observed. Upon reaching the terminal velocity of zirconia particles, these particles tend to accumulate in the upper part of the packed section: an incipient segregation of zirconia particles appears at the relatively high superficial gas velocities ($V_f > 9$ m/s).

4.4 Overall pressure drop in a three phase system

Eq. (28) shows that the overall pressure drop in a counter-current flow of coarse and dense particles, and a suspension of fine particles depends on the solids hold-ups, the voidage of packing and the interaction terms due to direct contact of each phase with the packing. Fig. 14 presents a comparison between the calculated values of the overall pressure drop obtained from Eq. (28) and the experimental results obtained in the pilot-scale unit of the packed gas-solid-solid contactor: for a given sand flow rate, all results are located in the vicinity of the bisecting line, irrespectively of a zirconia flow rate.

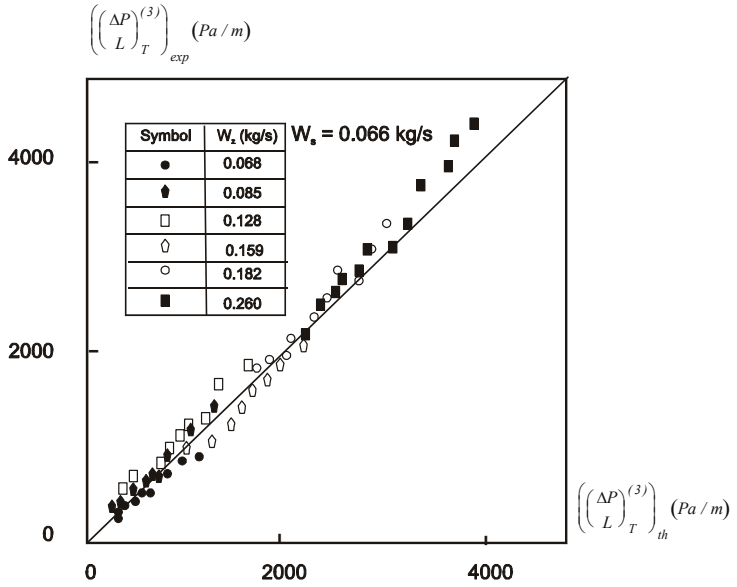

Fig. 14 Comparison between predicted values of the overall pressure drop in a tri-phase system those obtained from direct measurements on pilot-scale unit

5 Models for predicting particle-packing walls

Because of their trajectories, particles hit the column and packing walls. These collisions have a random character: the velocities of the particles after collisions cannot be anticipated before the collisions. Such collisions generate a certain scatter in particle velocities, which promotes collisions between particles. Collisions that involve energy dissipation are usually analyzed by relating the normal component of incident and separation velocities to a coefficient of restitution. Newton was first commented on this relationship and reported values of 5/9 for iron spheres, 5/9 for compressed wool, and 15/16 for glass spheres at moderate speeds [27]. More recently, Kharaz et al. [28] and Gorham et al. [29] showed that, in the case of 5-mmm aluminum-oxide spheres rebounding from a thick soda-lime glass anvil, the value of the normal coefficient of restitution varies slightly (of the order of 1 %) with the impact angle. The value of the tangential coefficient of restitution drops from 0.793 to 0.594 when the impact angle increases from 2 to 15 degrees, and then increases from 0.594 to 0.976 when the impact angle increases from 15 to 85 degrees. The expression for particle-packing walls interactive forces is formulated by examining the collisions between the particles and the external and internal walls of the packing. Fig. 15 shows two types of collisions: frontal and lateral collisions.

5.1 Lateral collisions

The axial momentum loss of particle "*p*" colliding with the packing walls can be written as follows:

$$\left(\Gamma_{pw}\right)_x^{lat} = m_p\left[\left(V_p^{lat}\right)_x^{ref} - \left(V_p^{lat}\right)_x^{inc}\right]. \tag{34}$$

The reflecting velocity $\left(V_p^{lat}\right)_x^{ref}$ in the axial direction is related to the incident velocity $\left(V_p^{lat}\right)_x^{inc}$ by the coefficient of restitution, λ_x^{lat}, which is usually defined as an

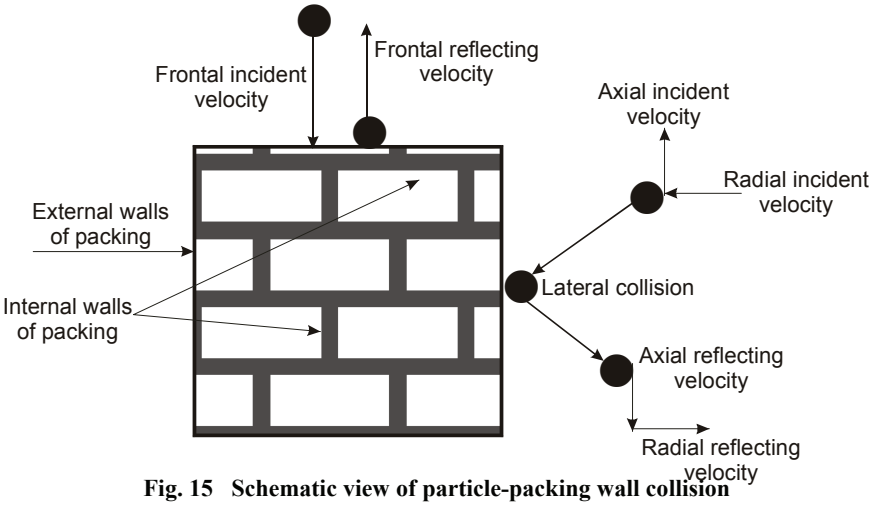

Fig. 15 Schematic view of particle-packing wall collision

empirically determined constant of proportionality that relates normal components of relative incident and rebound velocities for contact points of colliding rigid bodies. Hence, Eq. (34) becomes:

$$\left(\Gamma_{pw}\right)_x^{lat} = m_p \left(\lambda_x^{lat} - 1\right)\left(V_p^{lat}\right)_x^{inc} . \tag{35}$$

The reflecting velocities in the axial and radial directions are related to the incident velocities by the coefficient of restitution, and are, respectively:

$$\left(V_p^{lat}\right)_x^{ref} = \lambda_x \left(V_p^{lat}\right)_x^{inc} \tag{36}$$

and

$$\left(V_p^{lat}\right)_r^{ref} = -\lambda_r \left(V_p^{lat}\right)_r^{inc} . \tag{37}$$

The mean axial particle velocity, $\left(V_p^{lat}\right)_x^{vw}$, in the vicinity of the walls is proportional to the time spent in the vicinity of the packing walls. In other words, it is inversely proportional to the radial incident and reflecting velocities. The equation describing this mean axial particle velocity must therefore take into account the dynamic state of the particle "*p*" before and after collisions, viz.:

$$\left(V_p^{lat}\right)_x^{vw} = \left(\frac{dt_p^{inc}}{dt_p^{inc} + dt_p^{ref}}\right)\left(V_p^{lat}\right)_x^{inc} + \left(\frac{dt_p^{ref}}{dt_p^{inc} + dt_p^{ref}}\right)\left(V_p^{lat}\right)_x^{ref} \tag{38}$$

where dt is the residence time of the particle p (or a solid phase) in the vicinity of the walls:

$$dt = dt_p^{inc} + dt_p^{ref} , \tag{39}$$

where $$dt_p^{inc} = \frac{d\delta}{\left(V_p^{lat}\right)_r^{inc}} \quad \text{and} \quad dt_p^{ref} = \frac{d\delta}{\left(V_p^{lat}\right)_r^{ref}} \tag{40}$$

$d\delta$ is the thickness of parietal collision layer.

Combining Eqs. (38) and (40) with Eqs. (36) and (37) gives:

$$\left(V_p^{lat}\right)_x^{vw} = \frac{\lambda_x^{lat} - \lambda_r^{lat}}{1-\lambda_r^{lat}}\left(V_p^{lat}\right)_x^{inc}. \tag{41}$$

During collisions, the momentum lost by the particle is given as:

$$\left(\Gamma_{pw}\right)_x^{lat} = m_p\left(\left(V_p^{lat}\right)_x^{ref} - \left(V_p^{lat}\right)_x^{inc}\right) = m_p\left(\lambda_x^{lat} - 1\right)\left(V_p^{lat}\right)_x^{inc}. \tag{42}$$

Combining Eq. (42) with Eq. (41) results in:

$$\left(\Gamma_{pw}\right)_x^{lat} = m_p\left\{\frac{\left(\lambda_x^{lat} - 1\right)\left(1-\lambda_r^{lat}\right)}{\lambda_x^{lat} - \lambda_r^{lat}}\right\}\left(V_p^{lat}\right)_x^{vw}. \tag{43}$$

The particles-packing walls interactive forces are given by multiplying the momentum lost by the collision frequency per unit volume, which is proportional $\left(k_v\right)$ to the solid volumetric concentration in the vicinity of walls:

$$F_{pw}^{lat} = k_v \rho_p\left\{\frac{\left(\lambda_x^{lat} - 1\right)\left(1-\lambda_r^{lat}\right)}{\lambda_x^{lat} - \lambda_r^{lat}}\right\}\left(V_p^{lat}\right)_x^{vw}\left(\alpha_p^{lat}\right)_x^{vw}. \tag{44}$$

Note that the above dependence of F_{pw}^{lat} on $\left(\alpha_p^{lat}\right)_x^{vw}$ and the solid particle velocity at the walls holds even if the particles are not actually colliding with the packing walls but only sliding along it in continuous contact. Now, assuming that the concentration and velocity profiles of the solid phases are uniform, the local variables can be replaced by the average variables, and Eq. (44) becomes:

$$\bar{F}_{pw}^{lat} = k_v \rho_p\left\{\frac{\left(\lambda_x^{lat} - 1\right)\left(1-\lambda_r^{lat}\right)}{\lambda_r^{lat} - \lambda_x^{lat}}\right\}\bar{V}_p\bar{\alpha}_p. \tag{45}$$

5.2 Frontal collisions

In frontal collisions, the momentum variation of particles "*p*" in the axial direction is given by:

$$\left(\Gamma_{pw}\right)_x^{fr} = -\ m_p\left(1+\lambda_x^{fr}\right)\left(V_p^{fr}\right)_x^{inc} \tag{46}$$

and the frequency of frontal collisions $\left(\Pi_{pw}^{fr}\right)$ is given by:

$$\Pi_{pw}^{fr} = \frac{\left(V_p^{fr}\right)_x^{inc}}{L_p}, \tag{47}$$

where L_p is the mean path between two successive collisions. As suggested by Gidaspow [26], by the application of the kinetic theory of dilute gases, the mean free path concept for spherical particles is determined as follows:

$$L_p = \frac{1}{6\sqrt{2}} \frac{d_p}{\alpha_p} . \tag{48}$$

Figs. 16 and 17 summarize the possible values of the mean-free paths corresponding to the frontal collisions have undergone by solid particles. It shows clearly that for a given solid flow rate the mean path between two successive collisions increases with the superficial gas velocity in the case of the air-sand system (co-current flow) whereas it decreases for the air-zirconia system (counter-current flow). As shown in Figs. 16 and 17, the results are well fitted with a regression equation of two- parameter power-type for the air-sand systems $\left(L_s = aV_f^b\right)$, and regression equation of two-parameter single exponential decay-type $\left(L_z = a' \ e^{-b'V_f}\right)$ for the air-zirconia system. These values are in the same order of magnitude as those obtained using high-speed camera records which show that the distance between two successive collisions varies approximately from 10 to 25 mm. Therefore, the force due to frontal collisions can be expressed as:

$$F_{pw}^{fr} = -\rho_p \left(1+\lambda_x^{fr}\right)\left(\alpha_p^{fr}\right)_x \frac{\left[\left(V_p^{fr}\right)_x^{inc}\right]^2}{L_p} . \tag{49}$$

Since the dynamic effects of lateral and frontal collisions are additive, the total average force attributed to the overall collisions can be expressed as follows:

$$\bar{F}_{iw} = \left\{\left[k_v \frac{\left(\lambda_x^{lat}-1\right)\left(1-\lambda_r^{lat}\right)}{\lambda_r^{lat}-\lambda_x^{lat}}\right] - \left[\left(1+\lambda_x^{fr}\right)\frac{\bar{V}_i}{L_i}\right]\right\}\rho_i \bar{\alpha}_i \bar{V}_i , \tag{51}$$

where *i* corresponds to the solid phase, either sand or zirconia.

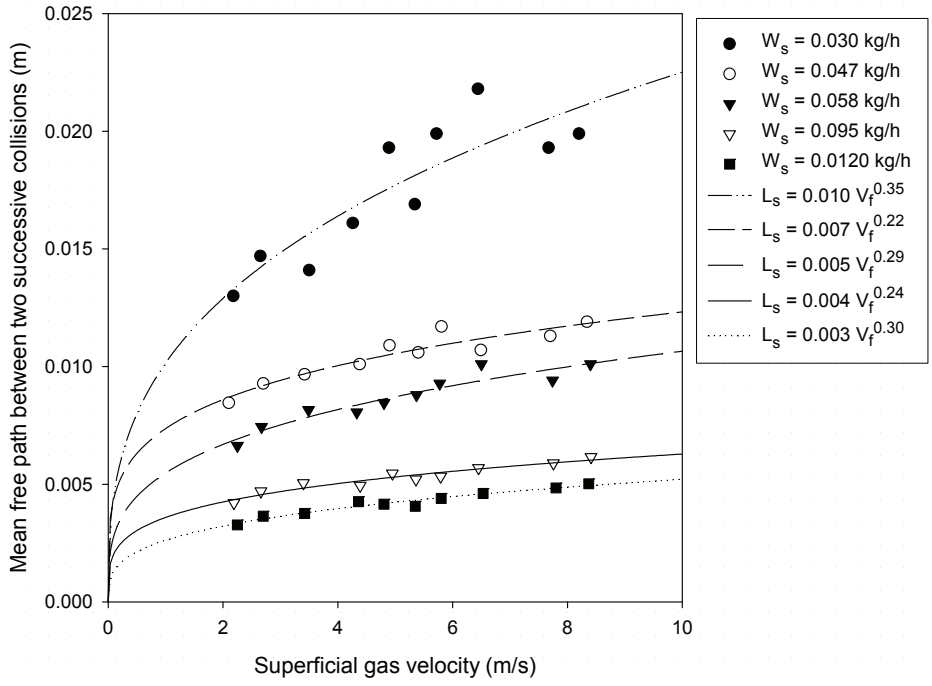

Fig. 16 Mean free path of two successive collisions: air-sand system

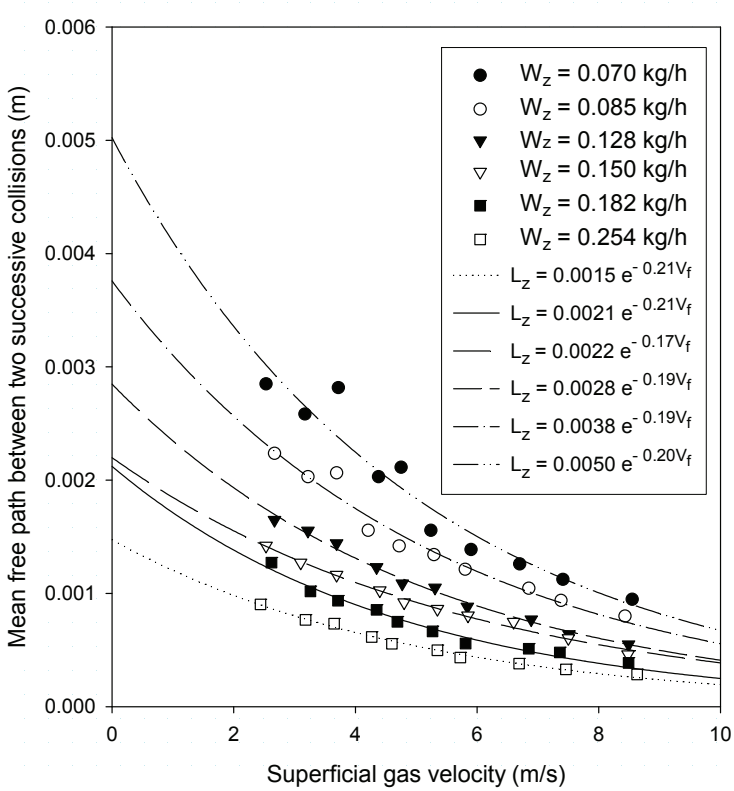

Fig. 17 Mean free path of two successive collisions: air-zirconia system

Eq. (51) shows the important effect of the solids mass flow rate of on the calculation of the forces attributable to particle-wall collisions. The effect of the gas phase appears through the average velocity of solids, which is directly affected by the gas superficial velocity. However, if the frontal collisions are elastic in the axial or radial direction, i.e. $\lambda_x^{lat} = 1$ or $\lambda_r^{lat} = 1$, the first term of Eq. (51) will be zero. Eq. (51) shows also that lateral collisions cannot be identical in axial and radial directions.

Figs. 18 and 19 show a comparison of the values of $\bar{F}_{ws}^{(1)}$ and $\bar{F}_{wz}^{(2)}$, as calculated with Eqs. (31) and (32), with those calculated by using Eq. (51). Based on this comparison, it can be seen that the coefficient of restitution has a remarkable effect on the calculated values of $\bar{F}_{ws}^{(1)}$ and $\bar{F}_{wz}^{(2)}$. When $\lambda_r^{lat} = 0$ and $0.25 \le \lambda_x^{lat} \le 0.50$, an acceptable agreement is observed between the values resulting from Eq. (51) and those obtained experimentally: globally, the collisions between solid particles and packing walls are thus inelastic. In addition, the analysis of results demonstrates insignificant contribution of frontal collisions to the overall particle-packing interactive force.

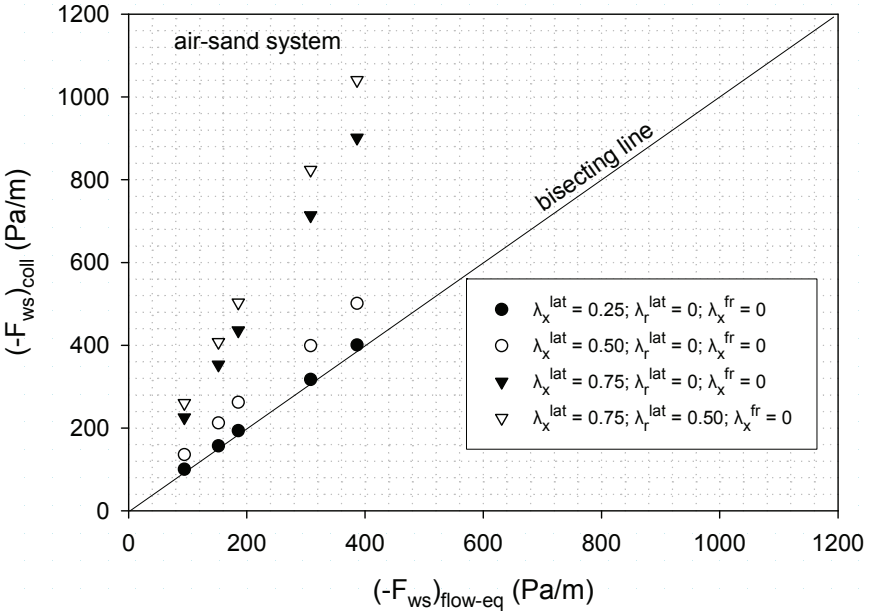

Fig. 18 Comparison of values of calculated $\overline{F}_{ws}^{(1)}$ using collision model with those calculated by Eq. (51)

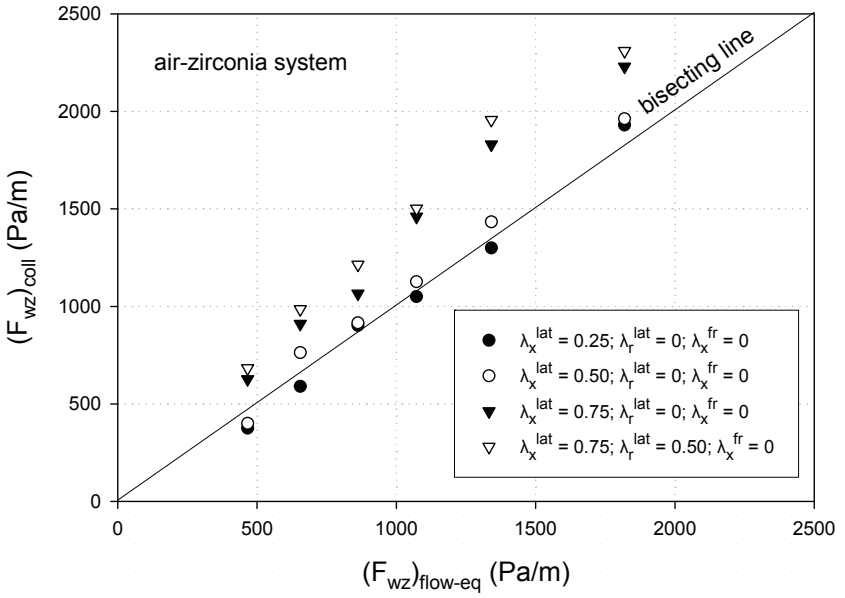

Fig. 19 Comparison of values of calculated $\overline{F}_{wz}^{(2)}$ using collision model with those calculated by Eq. (51)

6 Concluding remarks

This work demonstrates that it is possible to formulate equations describing the direct contact mechanism of gas-solid mixtures without major assumptions. Although this theoretical analysis assumes a low volume for the particle fraction in the suspension, it takes into account the first effects of particle interaction. The mechanistic analysis presented in this paper indicates that the hydrodynamic behavior of a dilute three-phase system can be described on the basis of the hydrodynamic features of two two-phase systems (Fig. 20). Thus, this study contributes to hydrodynamic analyses of dilute gas-solid suspensions and may give an indication on the expected physical mechanisms occurring in more concentrated suspensions. The important role of particle-particle interaction is to determine a particle velocity and thereby a "particle pressure" that resists the formation of particle density variations.

In order to focus on the role of hydrodynamic parameters, we have drawn a flow diagram based on particle-particle interaction. An important aspect of this diagram is that it reveals how the range of this interaction is limited. However, it is interesting to note that additional effects such as electrostatic and Van der Walls forces have not been included (the solid particles used belong to Class B of Geldart's classification of powders). Moreover, these particles are sufficiently large that the effects of Brownian motion become negligible (d_p o 1 μm).

The most important aspect of this theoretical approach is the presence of interfaces separating the various phases. Its limitations must also be borne in mind: it can be used only for dilute suspensions.

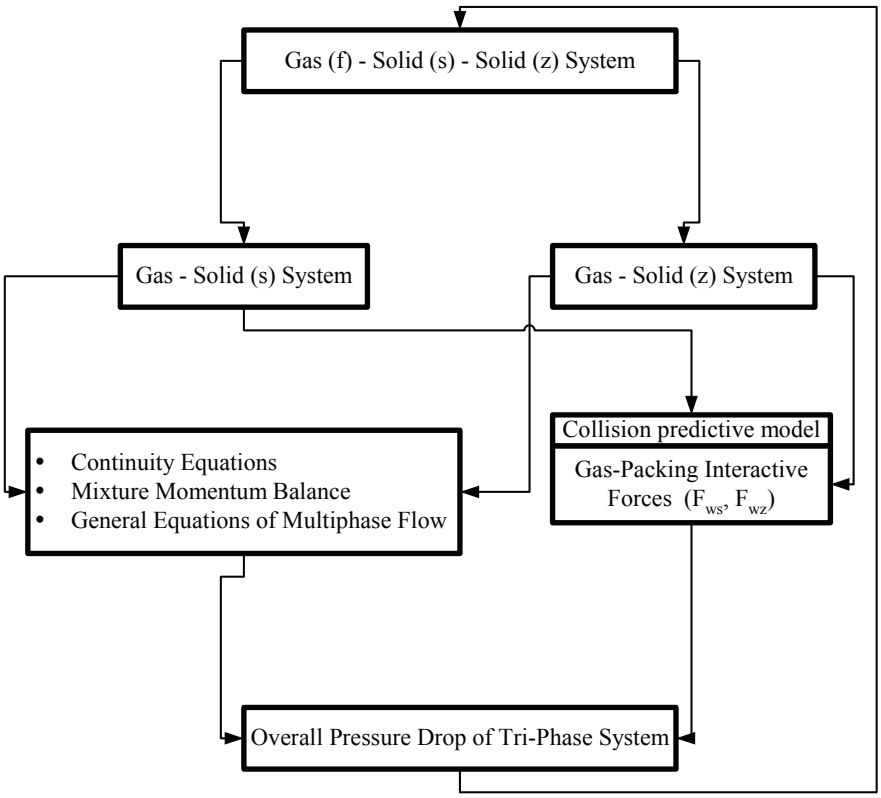

Fig. 20 Hydrodynamics of dilute tri-phase system: Simplified approach

References

[1] R.J. Lee and L.S. Fan, The effect of solid interaction forces on pneumatic handling of sorbent powders, *AIChE. J.*, 39 (1993) 1018-1029.

[2] H.Y. Xie, The role of interparticle forces in the fluidization of fine particles, *Powder Technol.*, 94 (1997) 99-108.

[3] R.C. Senior and J.R. Grace, Integrated particle collision and turbulent diffusion model for dilute gas-solid suspensions, *Powder Technol.*, 96 (1998) 48-78.

[4] C. Fyhr and A. Rasmuson, Mathematical model of a pneumatic conveying dryer, *AIChE. J.*, 43 (1997) 2889-2902.

[5] M.L. Passos and A.S. Mujumdar, Effect of cohesive forces on fluidized and spouted beds of wet particles, *Powder Technol.*, 110 (2000) 222-238.

[6] H. Wang, Measurement and analysis of particle-particle interaction in dilute vertical solids Transport, M.Sc. Dissertation, Institute of Technology of Chicago, USA, 1981.

[7] H. Arastoopour, S.C. Lin and S.A. Weil, Analysis of vertical pneumatic conveying of solids using multi-phase models", *AIChE J.*, 28 (1982) 467-473.

[8] H. Arastoopour, C.H. Wang and S.A. Weil, Particle-particle interaction force in a dilute gas-solid system", *Chem. Eng. Sci.*, 37 (1982) 1379-1386.

[9] H. Arastoopour and J.H. Cutchin, Measurement and analysis of particle-particle interaction in a concurrent flow of particles in a dilute gas-solid system", *Chem. Eng. Sci.*, 40 (1985) 1135-1143.

[10] L.S. Fan, M. Toda and S. Satija, Hold-up of fine particles in the packed dense bed of the multisolid pneumatic transport bed, *Powder Technol.*, 36 (1983) 107-114.

[11] S. Satija and L.S. Fan, Terminal velocity of dense particles in the multi-solid pneumatic transport bed, *Chem. Eng. Sci.*, 40 (1985) 259-267.

[12] E. Saatdjian and J.F. Large, Heat transfer simulation in a raining packed bed exchanger, *Chem. Eng. Sci.*, 40 (1985) 693-697.

[13] E. Saatdjian and J.F. Large, Heat transfer in a counter current gas-solid packed column, *J. Heat Transfer*, 110 (1988) 385-389.

[14] J.E. Gwyn, Interactive forces in contraflow ball/particulate fluidized bed, *Fluidization V*, Proc. of the fifth Eng. Found. Conference on Fluidization, 321-328 (1986)..

[15] D. Gidaspow, Hydrodynamics of fluidization and heat transfer: Supercomputer modeling, *Appl. Mech. Rev.*, 39 (1986) 1-23.

[16] R.A. Bagnold, Experiments on a gravity-free dispersion of large solid spheres in a Newtonian fluid under shear, *Proc. Roy. Soc.*, A225 (1954) 49-63.

[17] A. Fortier, Mécanique des Suspensions (*Mechanics of suspensions*), Masson et Cie. Ed., Paris, 1967, pp. 79-95.

[18] J. Ding and D. Gidaspow, A bubbling fluidization model using kinetic theory of granular flow, *AIChE. J.*, 36 (1990) 523-538.

[19] J.L. Sinclair, Hydrodynamic modeling, in Circulating Fluidized beds, Eds. J.R. Grace, A.A. Avidan and T.M. Knowlton, Chapman and Hall, 1997, pp. 149-180.

[20] Y. Molodstof and D.W. Muzyka, General probabilistic multi phase flow equations. for analyzing gas-solids mixtures, *Int. J. Eng. Fluid Mech.*, 2 (1989) 1-24.

[21] M. Benali and K. Shakourzadeh-Bolouri, The gas-solid-solid packed contactor: Hydrodynamic behaviour of trickle flow of coarse and dense particles in counter-current with a suspension of fine particles", *Int. J. Multiphase Flow*, 20 (1994) 161-170.

[22] Benali, M., K. Shakourzadeh-Bolouri and J.F. Large, "Hydrodynamic characterization of dilute suspensions in the gas-solid-solid packed contactor, *Fluidization VII*, Brisbane, Australia, 1992.

[23] A. Einstein, Eine neue bestimmung der molekul-dimensionen (*A New determination of molecular dimensions*), *Ann. Phys.*, 19 (1906) 289-290.

[24] A. Einstein, Berichtigung zu meiner artbeit: Eine neue bestimmung der molekuldimensionen (*Repair theory: An new determination of molecular dimensions*), *Ann. Phys.*, 34 (1911) 591-592.

[25] D.J. Jeffrey and A. Acrivos, The rheological properties of suspensions of rigid particles, *AIChE. J.*, 22 (1976) 417-432.

[26] D. Gidaspow, Multiphase flow and fluidization, Chapter 9, Academic Press, 1994, pp. 239-296.

[27] L. Landau and E. Lifchitz, Physique théorique: Mécanique quantique (*Theoretical physics: Quantum mechanics*), MIR, Moscow, 2nd Edn., 1988.

[28] A.H. Kharaz, D.A. Gorham and A.D. Salman, An experimental study of the elastic rebound of spheres, *Powder Technol.*, 120 (2001) 281-291.

[29] D.A. Gorham and A.H. Kharaz, The measurement of particle rebound characteristics, *Powder Technol.*, 112 (2000) 193-202.

Насадочный контактор «газ – твердое – твердое»: механический и макроскопический анализ взаимодействующих сил

Марзук Бенали

Госфирма КАНМЕТ, Центр энерготехнологий, Варенн, Канада

Ключевые слова и фразы: взаимодействующие силы; насадочный контактор; прямой контакт «газ – твердое»; разбавленная суспензия «газ – твердое».

Аннотация: Взаимодействующие силы между тремя фазами (газ, тонкие частицы, крупные и плотные частицы) управляют прямым механизмом контакта, который действует в насадочном контакторе «газ – твердое – твердое». Используя уравнения неразрывности и импульса, эти взаимодействующие силы определяются как функции общего перепада давления, средней динамической удерживающей способности твердых частиц и физических свойств твердых частиц, газа и регулярной насадки. Предложена модель столкновения «частицы – насадка»; чтобы объяснить возникновение и физическое происхождение этих взаимодействующих сил, измерить их и предсказать общий перепад давления в трехфазной системе.

Gitterungseinschalter "Gas – Hartes - Hartes": mechanische und makroskopische Analyse der zusammenwirkenden Kräfte

Zusammenfassung: Die zusammenwirkenden Kräfte zwischen drei Phasen (Gas, die feinen Teilchen sowohl die grossen als auch dichten Teilchen) verwalten den direkten Mechanismus des Kontaktes, der im Gitterungseinschalter "Gas – Hartes – Hartes" funktioniert. Benutzend die Gleichungen der Kontinuität und des Impulses, werden diese zusammenwirkenden Kräfte als die Funktionen der gemeinen Druckdifferenz, der mittleren dynamischen festhaltenden Fähigkeit der festen Teilchen und der physikalischen Eigenschaften der harten Gasteilchen und der regelmässigen Gitterung bestimmt.Es ist das Modell der Kollision des Teilchens – der Gitterung angeboten, um die Entstehung und die physikalische Abstammung dieser zusammenwirkenden Kräfte zu erklären, sie zu messen und die gemeine Druckdifferenz im dreiphasigen System vorauszusagen.

Contacteur Garni Gaz-Solide-Solide: analyse mécanique et macroscopique des forces d' interaction

Résumé: Les forces d'interaction entre les trois phases en présence (gaz, particules fines et les particules grosses et denses) régissent le mécanisme de contact direct se produisant au sein du Contacteur Garni Gaz-Solide-Solide. En utilisant les équations de continuité et d'impulsion, ces forces d'interaction sont déduites comme étant des fonctions de la perte de charge globale, de la rétention dynamique des solides et des propriétés physiques des solides, du gaz et du garnissage ordonné. Le modèle de collisions particules-parois du garnissage a été proposé pour interpréter l'existence et les origines physiques de ces forces d'interaction ainsi que pour les quantifier et prédire la perte de la charge globale au sein du système à trois phases.